Acta Biomaterialia 170 (2023) 543–555

Contents lists available at ScienceDirect

Acta Biomaterialia

journal homepage: www.elsevier.com/locate/actbio

Full length article

High-precision targeting and destruction of cancer-associated PDGFR-β^+ stromal fibroblasts through self-assembling, protein-only nanoparticles

Eric Voltà-Durán[a,b,c,1], Lorena Alba-Castellón[c,d,e,1,*], Naroa Serna[a,b,c,2], Isolda Casanova[c,d,e], Hèctor López-Laguna[a,b,c], Alberto Gallardo[d,g], Alejandro Sánchez-Chardi[f,3], Antonio Villaverde[a,b,c,*], Ugutz Unzueta[c,d,e], Esther Vázquez[a,b,c], Ramón Mangues[c,d,e,*]

[a] Institut de Biotecnologia i de Biomedicina, Universitat Autònoma de Barcelona, Bellaterra, Barcelona 08193, Spain
[b] Departament de Genètica i de Microbiologia, Universitat Autònoma de Barcelona, Bellaterra, Barcelona 08193, Spain
[c] CIBER de Bioingeniería, Biomateriales y Nanomedicina (CIBER-BBN), Spain
[d] Biomedical Research Institute Sant Pau (IIB Sant Pau), Barcelona 08041, Spain
[e] Josep Carreras Leukaemia Research Institute, Barcelona 08025, Spain
[f] Departament de Biologia Evolutiva, Ecologia i Ciències Ambientals, Facultat de Biologia, Universitat de Barcelona, Av. Diagonal 643, Barcelona 08028, Spain
[g] Department of Pathology, Hospital de la Santa Creu i Sant Pau, Barcelona 08025, Spain

ARTICLE INFO

Article history:
Received 25 May 2023
Revised 30 August 2023
Accepted 1 September 2023
Available online 6 September 2023

Keywords:
Nanoparticles
Protein materials
Cell targeting
Cancer
Drug delivery
Precision medicines
Nanomedicine

ABSTRACT

The need for more effective and precision medicines for cancer has pushed the exploration of new materials appropriate for drug delivery and imaging, and alternative receptors for targeting. Among the most promising strategies, finding suitable cell surface receptors and targeting agents for cancer-associated platelet derived growth factor receptor β (PDGFR-β)$^+$ stromal fibroblasts is highly appealing. As a neglected target, this cell type mechanically and biologically supports the growth, progression, and infiltration of solid tumors in non-small cell lung, breast, pancreatic, and colorectal cancers. We have developed a family of PDGFR-β-targeted nanoparticles based on biofabricated, self-assembling proteins, upon hierarchical and iterative selective processes starting from four initial candidates. The modular protein PDGFD-GFP-H6 is well produced in recombinant bacteria, resulting in structurally robust oligomeric particles that selectively penetrates into PDGFR-β^+ stromal fibroblasts in a dose-dependent manner, by means of the PDGFR-β ligand PDGFD. Upon *in vivo* administration, these GFP-carrying protein nanoparticles precisely accumulate in tumor tissues and enlighten them for IVIS observation. When GFP is replaced by a microbial toxin, selective tumor tissue destruction is observed associated with a significant reduction in tumor volume growth. The presented data validate the PDGFR-β/PDGFD pair as a promising toolbox for targeted drug delivery in the tumor microenvironment and oligomeric protein nanoparticles as a powerful instrument to mediate highly selective biosafe targeting in cancer through non-cancer cells.

Statement of significance

We have developed a transversal platform for nanoparticle-based drug delivery into cancer-associated fibroblasts. This is based on the engineered modular protein PDGFD-GFP-H6 that spontaneously self-assemble and selectively penetrates into PDGFR-β^+ stromal fibroblasts in a dose-dependent manner, by means of the PDGFR-β ligand PDGFD. *In vivo*, these protein nanoparticles accumulate in tumor and when incorporating a microbial toxin, they destroy tumor tissues with a significant reduction in tumor volume, in absence of side toxicities. The data presented here validate the PDGFR-β/PDGFD pair as a fully versatile toolbox for targeted drug delivery in the tumor microenvironment intended as a synergistic treatment.

* Corresponding authors at: CIBER de Bioingeniería, Biomateriales y Nanomedicina (CIBER-BBN), Spain.
E-mail addresses: LAlba@santpau.cat (L. Alba-Castellón), antoni.villaverde@uab.cat (A. Villaverde), rmangues@santpau.cat (R. Mangues).
[1] These authors contributed equally to this work.
[2] Present address: Nanoligent SL, Edifici Eureka, Universitat Autònoma de Barcelona, Bellaterra, 08193 Barcelona, Spain.
[3] Present address: Oficina de Sostenibilitat, Edifici L, Universitat Autònoma de Barcelona, Bellaterra, Barcelona 08193, Spain.

https://doi.org/10.1016/j.actbio.2023.09.001
1742-7061/

1. Introduction

Cancer represents a leading cause of death worldwide and an unmet clinical problem [1]. It is so despite the substantial economic and human resources invested in anti-tumor drug discovery and the diversity of innovative therapeutic approaches and emerging materials intended for more effective drug delivery that are currently under evaluation [2–6]. The generic lack of selectivity and high toxicity of most chemical drugs, the development of drug resistance and relapse and the multiple facets that support cancer development and progression make this goal especially complex. Increasing drug selectivity for target cells through smarter and selective drug vehicles and identifying complementary therapeutic targets should both support significant steps towards successful cancer therapies. In the context of these non-exclusive alternatives, high precision drug delivery is being explored mainly by the refinement of nanomedical tools [7–13] and by developing biocompatible materials within the nanoscale as drug carriers. Their building blocks are to be functionalized with specific ligands of overexpressed tumoral markers for selective cytotoxic drug delivery and the consequent cell destruction, in a selective way [11,14–16]. Based on such functionalization, oligomeric nanoparticles benefit from the resulting cooperativity in receptor binding, enhanced endosomal engulfment and higher cell penetrability compared to monomeric ligands [17–20]. Metastatic cancer stem cells are particularly appealing targets for high precision nanomedicines as they are the origin of metastases, the main cause of patients' death. So far, despite being theoretically promising, attempts of selectivity in cancer nanomedicines have not generically reached accumulation in target tissues, being over 1-2 % of the administered material [21,22]. Further, many nanoscale materials, because of their physicochemical properties or their natural interactivity with biological receptors are in fact retained in liver or phagocyted [23–25], precluding the desired biodistribution of the carrier and the payload drug. An interesting exception is the engineering of self-assembling tumor-targeted modular proteins, that follow a highly desired tumor biodistribution [26–28] and which in some cases show values of tumor accumulation, upon systemic administration, over 85 % of the total observed signal [29,30].

On the other hand, the identification of alternative or complementary targets for selective cell killing offers promising routes to designing innovative drugs [31]. Looking at those other potential strategies, stroma refers to the tissue that surrounds epithelial cancer cells, including extracellular matrix, endothelial cells, immune cells and fibroblasts, which modulate and participate in cancer development. Among these elements, fibroblasts, synthesize and remodel the extracellular matrix being then responsible for the cancer tissue architecture and structural properties [32]. Fibroblasts are also responsible for the production of growth factors and cytokines that will be secreted within the tumor [33], supporting its development [32,34]. In particular, a specific subpopulation of this cell type, namely platelet-derived growth factor receptor β (PDGFR-β)-expressing fibroblasts are positively involved in cancer progression and its infiltration in tumors compromises patient survival, especially in non-small cell lung, breast, pancreatic and colorectal cancer [35–38]. PDGFR-β is a transmembrane protein, member of the family of Tyr kinases that participates in cell differentiation, migration and proliferation processes in several neoplasias [39]. Importantly, its expression levels in cancer-associated fibroblasts (CAFs) correlates with bad prognosis, relapse and drug resistance in several types of cancer [40–44]. Therefore, stromal PDGFR-β^+ fibroblasts are a pivotal, highly interesting cell type for imaging, drug delivery or selective destruction in the context of cancer therapies [45]. Despite the robust data supporting PDGFR-β^+ fibroblasts as targets in cancer therapies [35,39,42,46,47], the modest explorations have been so far limited to interfere signaling [48], but appropriate drugs or drug vehicles have not been yet developed and this type of approach has been essentially neglected.

In the present study, we have combined structural concepts from biomaterial design and self-assembling and from cell-targeted cancer nanomedicines based on ligand-receptor pairs, with the potential use of PDGFR-β-expressing stromal fibroblasts as targets for anticancer therapies, either as single agents or in combination with additional targeted drugs. Taking the concept of modular proteins as versatile and convenient materials for bio-inspired and clinically-oriented uses [49–60], we have generated protein-only nanoparticles based on self-assembling building blocks and targeted to cell-surface receptors of these cells. These materials, produced by simple and fully scalable biofabrication processes, have been successfully validated here as highly selective targeting agents which allow internalization in PDGFR-β^+ fibroblasts, both in cell culture and *in vivo*, using multiple analytical procedures. By incorporating a potent microbial toxin, the targeted nanoparticles promote a precise and selective destruction of tumor in an animal subcutaneous model of colorectal cancer, resulting in reduction of tumor volume growth. Altogether, the obtained data fully supports the concept of selective drug carriers based on nanoscale protein materials to target the main architectonic agents in solid tumors for their further development and use in the clinical setting.

2. Experimental section

2.1. Protein description

Four peptide ligands of PDGFR-β were selected from literature and described hereafter. Platelet derived growth factor B (PDGFB) and platelet derived growth factor D (PDGFD) are both human ligands of PDFGR-β [61]. PDGFRP1 is a small cationic peptide isolated by phage display [62], while Z09591 is an anionic affibody also identified by phage display and commonly used for radiolabeling and imaging of PDGFR-β expression in different cancers [46,63,64].

2.2. Protein design, production, and purification

The sequences of four green fluorescent PDGFR-β targeted proteins and the PDGFR-β targeted nanotoxin PDGFD-NT-H6 were designed *in house* as codon-optimized genes and subcloned into pET22b plasmids using NdeI and HindIII restriction enzymes. Geneart (ThermoFisher) provided the recombinant plasmids. For fluorescent proteins, PDGFR-β targeted domains were placed at the N-terminus of each protein, followed by a flexible linker (GGSSRSS), the green fluorescent protein (GFP) and the hexa-histidine tag H6. The H6 tag allows both protein purification but it also promotes assembling through coordination with divalent cations [65]. For the nanotoxin, PDGFD was located at the N-terminus, followed by a furin cleavable site (GNRVRRSV) flanked by two flexible linkers (GGSSRSS), the catalytic domain of *Pseudomonas aeruginosa* exotoxin A (PE24), the H6 tag and the C-terminal subcellular location signal KDEL. The recombinant pET22b vectors were transformed into *Escherichia coli* by heat shock at 42 ºC for 45 s. PDGFRP1-GFP-H6 and Z09591-GFP-H6, lacking intramolecular or intermolecular disulfide bonds, were produced in BL21 (DE3), PDGFB-GFP-H6 in Origami B (BL21 DE3, OmpT$^-$, Lon$^-$, TrxB$^-$, Gor$^-$, Novagen), and PDGFD-GFP-H6 and PDGFD-NT-H6 in BL21 (DE3) previously engineered for the expression of sulfhydryl oxidase and DsbC [66,67] (kindly provided by Prof. A. de Marco).

Protein production was carried out at the optimal conditions for each candidate. In this sense, PDGFRP1-GFP-H6 and Z09591-GFP-H6 were produced overnight at 20 ºC and 250 rpm in Luria Broth (LB) supplemented with 100 µg mL $^{-1}$ ampicillin, upon addition of 1×10^{-4} M of isopropyl-β-d-thiogalactopyronaside (IPTG), at OD_{550nm} 0.6-0.8 units. PDGFB-GFP-H6 was produced overnight

at 16 ºC and 250 rpm in LB supplemented with 100 μg mL $^{-1}$ ampicillin, 12.5 μg mL $^{-1}$ tetracycline and 15 μg mL $^{-1}$ kanamycin, upon addition of 1×10^{-4} M IPTG, at OD_{550nm} 0.6-0.8 units. Cells were then harvested by centrifugation (15 min, 5000 *g*) and stored at -80 ºC. For protein purification, cells were resuspended in wash buffer (2×10^{-2} M Tris-HCl, 5×10^{-1} M NaCl, 1×10^{-2} M imidazole, pH 8.0) in presence of protease inhibitors (cOmplete EDTA-free, Roche Diagnostics) and disrupted in an EmulsiFlex-C5 system (Avestin) by 3 rounds at 8000 psi. The soluble fraction was then collected by centrifugation (45 min at 15000 g) and proteins purified by an immobilized metal affinity chromatography (IMAC) using a HisTrap HP column (GE Healthcare) in an ÄKTA pure system (GE Healthcare). Elution was achieved by a lineal increase of imidazole concentration (Elution Buffer, 2×10^{-2} M Tris-HCl, 5×10^{-1} M NaCl, 5×10^{-1} M imidazole, pH 8.0).

For PDGFD-GFP-H6 and PDGFD-NT-H6 protein production, bacteria were grown in LB supplemented with 100 μg mL $^{-1}$ ampicillin and 34 μg mL $^{-1}$ chloramphenicol at 37 ºC until OD_{550nm} reached 0.4-0.5 units. In that moment, the expression of sulfhydryl oxidase and DsbC was induced by adding 0.5 % (m/v) of L-arabinose and temperature was lowered to 30 ºC. 45 min later, temperature was lowered to 16 ºC (PDGFD-GFP-H6) or 20 ºC (PDGFD-NT-H6) and 1×10^{-3} M of IPTG was added to induce overnight expression. In both cases, cells were then harvested by centrifugation (15 min 5000 *g*) and an osmotic shock was performed to remove the metallophores from the periplasmic fraction [68]. For that, cells were first resuspended in a hypertonic solution (20 % sucrose, 1×10^{-3} M ethylenediaminetetraacetic acid (EDTA), 5×10^{-2} M 4-(2-hydroxyethyl)-1-piperazineethanesulfonic acid (HEPES), pH 7.9) and centrifuged (30 min, 7000 *g*, 4 ºC). Supernatant was discarded and cells were then resuspended in a hypotonic solution (5×10^{-3} M $MgSO_4$), placed 10 min at 4 ºC and subsequently centrifuged (15 min, 4500 *g*) to remove again the supernatant. Bacterial cells, now without periplasm, were finally resuspended in wash buffer in presence of protease inhibitors and stored at -80 ºC. Disruption and purification were carried out as stated for the other proteins. For comparison purposes, GFP-H6 was produced and purified as previously described [69].

2.3. Physicochemical characterization of proteins and protein materials

After purification, proteins were dialyzed against an appropriate solution, namely sodium carbonate (166 mM $NaCO_3H$, pH 8.0) for PDGFRP1-GFP-H6 and PDGFD-NT-H6 and sodium carbonate with salt (166 mM $NaCO_3H$, 333 mM NaCl, pH 8.0) for Z09591-GFP-H6, PDGFB-GFP-H6 and PDGFD-GFP-H6. A particular amount of $ZnCl_2$ was added to pure solutions of PDGFRP1-GFP-H6 (3:1 molar ratio, Zn^{2+}: Histidine residues in H6) and Z09591-GFP-H6 (1:1 molar ratio, Zn^{2+}: Histidine residues in H6) to promote protein assembling and nanoparticle formation. Protein purity and integrity was determined by sodium dodecyl sulfate polyacrylamide gel electrophoresis (SDS-PAGE), and western blot immunodetection using an anti-His (Santa Cruz Biotechnology) and an anti-GFP (Santa Cruz Biotechnology) antibody. The same molar amount was used for each protein. Protein concentration was determined by the Bradford assay (Bio-Rad). Dynamic light scattering (DLS) was used to determine the volume size distribution of each type of nanoparticle. Measurements were conducted in a Zetasizer Advanced Pro Blue (Malvern Instruments Limited) at 25 ºC and 633 nm (n=3) using a quartz cuvette. Also, the GFP fluorescence was evaluated in a Varian Cary Eclipse Fluorescence Spectrophotometer (Agilent Technologies). Protein concentration was set to 5 μM, the excitation wavelength to 488 nm and the emission recorded at 511 nm. For green fluorescent proteins, the percentage of intrinsic fluorescence was calculated in comparison to the non-targeted control GFP-H6. Protein stability in the *in vitro* culture media (Dulbecco's Modified Eagle Medium, DMEM, Gibco; supplemented with fetal bovine serum, FBS, Gibco) was measured by incubating the proteins at the maximum concentration used in *in vitro* experiments (1×10^{-3} M), for the maximum time of exposure (24 h) at 37 ºC, and separating the soluble and insoluble fractions by centrifugation (15 min, 15000 *g*). A protein electrophoresis gel, followed by an anti-His Western Blot, were finally performed. Size exclusion chromatography was used to reveal oligomeric status of PDGFB-GFP-H6 and PDGFD-GFP-H6. Both proteins were analyzed using Superdex 200 Increase 10-300 GL (Cytiva) operated at 4ºC, 0.5 mL/min, and 0.5 mg/mL (total amount 2.5×10^4 g). For PDGFD-GFP-H6, an additional analytical size exclusion chromatography was performed to discriminate among different populations of nanoparticles. For that, Superose 6 Increase 10-300 GL (Cytiva) was used under the same settings previously described for Superdex 200 Increase 10-300 GL.

2.4. Ultrastructural characterization

Nanoscale morphometry (size and shape) of the different protein nanoparticles was visualized at nearly native state with two rapid high-resolution imaging techniques. Drops of 5 μL of samples diluted at 0.2 μg mL^{-1} in its stock solution were deposited in silicon wafers (Ted Pella) and observed in a field emission scanning electron microscope (FESEM) Merlin (Zeiss) operating at 1 kV and equipped with an in-lens secondary electron detector. Drops of samples diluted at 0.2 μg mL^{-1} in its stock solution were negatively stained with 2 % uranyl acetate (Merck) in 400 mesh carbon-coated copper grids (Electron Microscopy Sciences) and observed in a transmission electron microscope (TEM) JEM 1400 (Jeol) operating at 80 kV and equipped with an Orius SC200 CCD camera (Gatan). Representative images of general fields and nanoparticles details were obtained at three magnifications.

2.5. Three-dimensional models and visualization

In silico three-dimensional structure prediction of the four PDGFR-β targeted modular proteins was performed using AlphaFold Colab. [70] ChimeraX software version 1.2 [71] was used then for their 3D structure visualization. GraphPad Prism 8 was used for graphics and statistical tests.

2.6. Cell lines and cell culture

Mouse Embryonic Fibroblasts (MEFs) and Mesenchymal Stem Cells (MSCs) were kindly provided by Prof. Antonio Garcia de Herreros [72,73]. MEFs, MSCs, and the mouse colorectal cancer cell line MC-38 (Kerafast) were cultured in Dulbecco's Modified Eagle's Medium (DMEM) 4.5g/L glucose, supplemented with 10 % Fetal Bovine Serum (FBS), 100 U/mL penicillin, 100 μg/mL streptomycin and 2 mM glutamine (Life Technologies) and incubated at 37°C and 5 % CO_2 in a humidified atmosphere.

2.7. Immunodetection

MEFs, MSCs and MC38 cells were plated in p100 dishes (3×10^5 cells/p100) and exposed to nanoparticles at different concentration (from 25 nM to 100 nM) for two time periods (1 h, 24 h). When indicated, cells were treated with 50 ng/mL of platelet derived growth factor B homodimer (PDGF-BB. Prepotech) 30 min prior exposure. Cells were washed with PBS, detached from the plate, and trypsinized (1 mg/ml trypsin, Life Technologies) for 15 min at 37°C to remove membrane binding of the nanoparticles. RIPA lysis buffer plus phosphatase and protease inhibitors (Roche) was used to obtain whole-cell extracts. Protein extracts were loaded

into 10-12 % acrylamide SDS-PAGE gel and transferred to a nitrocellulose membrane to detect GFP (Santa Cruz Technologies, sc-8334), PDGFR-β (Cell Signaling, 3169) and tubulin (Cell Signaling, 2148) by western blotting. Bands were visualized using ChemiDoc XRS+ imaging system (Bio-rad). Bands densitometry quantitation was performed with ImageJ software. All experiments were performed in triplicate.

2.8. Flow cytometry

Internalization of nanoparticles was quantified by GFP fluorescence signal using FACS Calibur (BD Biosciences). MEFs and MSCs were exposed at 25, 50, 100, 250, 500 and 1000 nM for 1 h or 24 h. After treatment, cells were washed with PBS, detached from the plate and trypsinized for 15 min at 37 ºC to eliminate non-internalized nanoparticle. Data were analyzed using the Flow Jo software and represented as mean fluorescence intensity (MFI) fold change with respect to buffer-treated cells. All experiments were performed in triplicate.

2.9. Confocal microscopy

For fluorescence microscopy, 1×10^4 cells were seeded on a coverslip in 24-well plate and exposed to 25, 50 or 100 nM nanoparticles for 1 h. When indicated, 50 ng/mL PDGF-BB (Prepotech) was added 30 min before exposure to assess competition. After incubation with nanoparticles, cells were washed, fixed with 4 % formaldehyde (ThermoFisher Scientific) and blocked with 3 % BSA. Then, nuclei were stained with DAPI and coverslips were mounted with ProLong™ Gold Antifade Mountant (ThermoFisher Scientific). Samples were visualized with SP5 Leica Microscopy.

2.10. Cell viability assay

Cell viability upon exposure to PDGFB-GFP-H6, PDGFD-GFP-H6 and PDGFD-NT-H6 was assessed with the Cell Proliferation Kit II (XTT) (Roche) according to the manufacturer's instructions. Briefly, 1×10^3 cells (MSCs) or 2×10^3 cells (MEFs, MC38) were seeded in 96-well plates and treated with different concentrations of PDGFB-GFP-H6 or PDGFD-GFP-H6 (250, 500 and 1000 nM) for 24 or 48h, or PDGFD-NT-H6 (100 nM) for 48 h. XTT reagent was added to the plate and further incubated at 37ºC for 4h, then absorbance, which directly correlates to the number of viable cells, was measured using a multi-well spectrophotometer (FLUOstar Optima, BMG Labtech). All experiments were performed in triplicate.

2.11. Mice and procedures for the administration of nanoparticles

All mice and procedures were carried out in accordance with the EU regulations on animal research and approved by Catalonia's Animal ethics committee (reference 9721). Eight-week-old female C57BL/6 were purchased from Charles River (France), housed in a specific pathogen-free (SPF) environment with sterile food and water *ad libitum*. The subcutaneous tumor model was generated by subcutaneous injection of 1 million MC-38 cells mixed with 0.5 million MEFs in the flank of the animal. For biodistribution assay, mice bearing tumors around 100-200 mm^3 were administrated intravenously with 200 µg of either PDGFB-GFP-H6 or PDGFD-GFP-H6 nanoparticles. This model and associated procedures have been previously validated in independent laboratories and shown to be robust for preclinical analyses [74–77]. Control animals were administrated with the stock buffer for nanoparticles. Animals were euthanized 2 h post-administration and an *ex vivo* measurement of fluorescence intensity (FLI) of tumors was performed using IVIS® Spectrum 200 (PerkinElmer). Tumors and organs were collected, fixed in 4 % formaldehyde solution and paraffin-embedded. Fluorescence intensity (FLI) data are expressed as average radiant efficiency and values have been calculated subtracting the FLI signal of buffer-treated mice to the FLI signal of nanoparticle treated animals. For antitumor evaluation, mice with 20-30 mm^3 tumors were randomised and intravenously administered with 1 mg/kg of PDGFD-NT-H6 nanotoxin or $NaHCO_3$, daily up to 7 doses. Tumors were harvested 72 h after last dose and measured *ex vivo* to calculate their volume. Tumour samples were paraffin-embedded for histological analysis. Tumor volume was calculated as $width^2$ x *length* x *0.5*. Mice were weighed twice a week since tumor implantation. Plasma obtained from whole cell blood extracted at the end point was used to detect Uric acid, Albumin, Creatinine (CRE) and transaminases (AST, ALT).

2.12. Histopathology

Paraffin-embedded 4 µm tissue sections were used for immunohistochemical analysis in DAKO Autostainer Link48 following the manufacturer's instructions. Antigen Retrieval was done in PT Link with pH high solution. The antibodies used were PDGFRβ (1:100, Cell Signaling 3169) and GFP (1:200, Santa Cruz sc-8334). Representative images were captured using an Olympus DP73 digital camera and processed with the Olympus CellD Imaging 3.3 software. Hematoxylin-eosin slides were scanned using Pannoramic Scan II (3D-Histech), and necrotic area quantification was performed using the measurement tool of Slide Viewer 2.5 software (3D-Histec). The percentage was calculated by dividing the necrotic area by the total tumor area.

2.13. Statistical analyses

Statistical analyses were performed using the GraphPad Prism 5 software (GraphPad Software, San Diego, California USA). Quantitative data were tested for both normal distribution and homogeneity of variances, using Kolmogorov-Smirnov and Levene's tests, respectively. Then, pairwise comparisons were made with *t*-Student or *U*-Mann-Whitney tests. Differences were considered statistically significant when p-values≤ 0.05.

3. Results and discussion

Four modular GFP-based proteins were designed for recombinant production, each carrying a specific PDFGR-β ligand, namely PDGFRP1, Z09591, PDGFB, or PDGFD (Fig. 1A). H6 tags were incorporated into the constructs to promote their self-assembly as regular protein-only nanoparticles [65], because of the interaction of the imidazole ring of the His residues with divalent cations [50,78]. *In silico* modeling of the constructs did not anticipate any structural constraint for the solvent display of the ligand or any steric impediment for the proper folding of the domains (Fig. 1B), as they were separated by a peptide linker (gray box, in Fig. 1A). The recombinant production of these constructs in bacteria rendered good yields of full-length protein species (between 5 and 120 mg/L), which, upon purification, resulted in discrete bands of the expected molecular weights (Fig. 1C). The integrity and high level of purity of all these constructs were further assessed by SDS-PAGE and independent Western blot analyses directed against alternative epitopes (Fig. S1A). The main biophysical profiles of the ligands and the resulting fusions, as well as the production and optimal storage conditions, are depicted in the Table S1. Upon dialysis, PDGFB- and PDGFD-based constructs rendered particulate materials of 16 and 26 nm (with a secondary minor peak of around 100 nm in the case of PDGFB-GFP-H6, Fig. 1D, Table S2), as expected for modular constructs based on H6-tagged GFP proteins with cationic

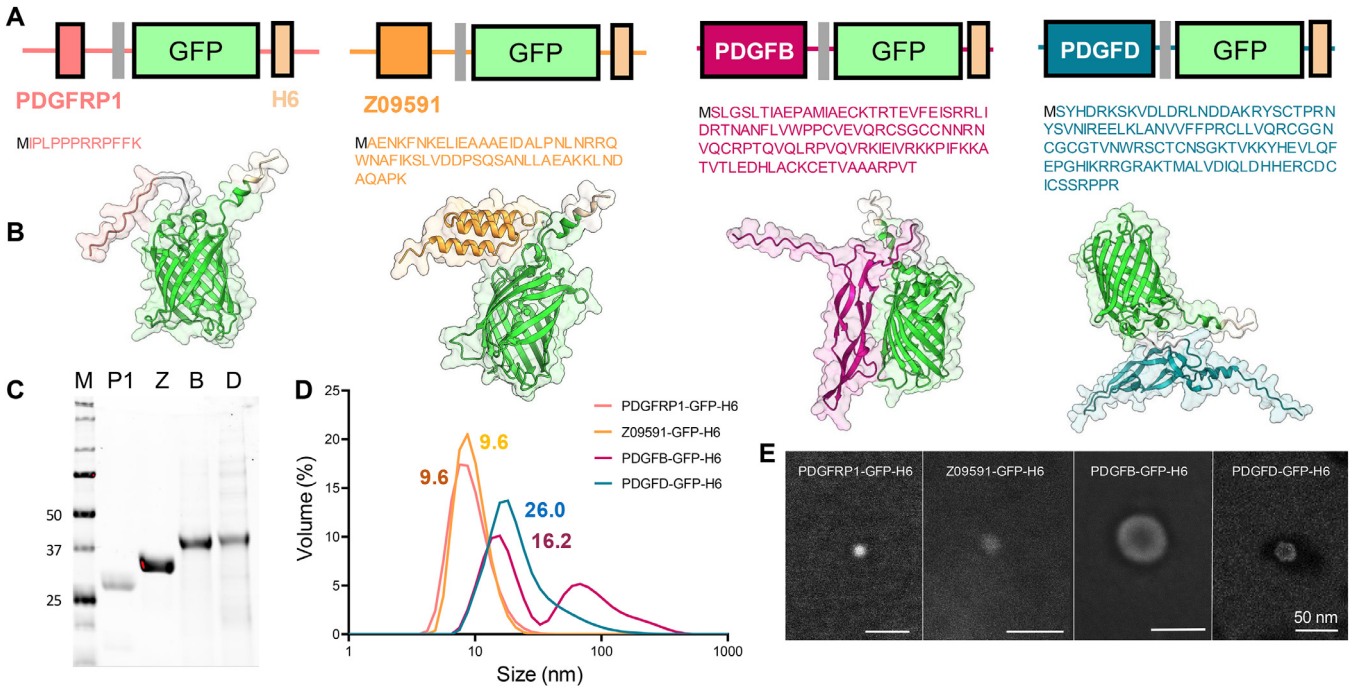

Fig. 1. Design and production of PDGFR-β targeted-proteins. (A) Modular disposition of each candidate, from the N-terminal (left) to the C-terminal (right) end. Modular proteins consist in a targeting peptide at the N-terminus (colored boxes), a flexible linker (GGSSGGS, grey box), the green fluorescent protein (GFP, green box) and a hexa-histidine tag (H6, orange box) at the C-terminus. The amino acid sequence of each targeting peptide is shown below. (B) Three-dimensional models of each candidate obtained by AlphaFold approach. Color code is as in panel A. (C) Protein gel electrophoresis, showing the obtained protein purity and the proteolytic integrity after affinity purification and further dialysis. P1 refers to PDGFRP1-GFP-H6 (29.7 kDa), Z to Z09591-GFP-H6 (34.6 kDa), B to PDGFB-GFP-H6 (40.5 kDa) and D to PDGFD-GFP-H6 (42.2 kDa). M indicates the marker lane, and the siding numbers the molecular mass of the markers expressed in kDa. (D) Particle size determined by DLS expressed in nm. Numbers indicate the mean peak size for every material. Additional data can be found in Table S2. (E) Representative FESEM images of isolated nanoparticles. The white bars represent 50 nm. Broader fields and TEM images for PDGFB-GFP-H6 and PDGFD-GFP-H6 are shown in the Fig. S2.

N-terminal domains [79]. As in the case of related protein constructs [80], the assembly was spontaneous and did not require additional cation supply. PDGFRP1-GFP-H6 and Z09591-GFP-H6 resulted in smaller nanoparticles of around 9 nm that were only formed when cationic Zn was added to the solution. All these materials were disassembled in the presence of detergent (Fig. S1B), confirming that they were oligomers formed by the recruitment of monomeric building blocks. Size exclusion chromatography data demonstrated the absence of monomeric populations of PDGFD-GFP-H6, whereas PDGFB-GFP-H6 presented multiple conformations (Fig. S1C), compatible with the results obtained by DLS (Fig. 1D). Interestingly, the analysis of PDGFD-GFP-H6 revealed the presence of protein nanoparticles with different sizes (Fig. S1D), which were hidden in the broad peak obtained by DLS. In this regard, size exclusion chromatography demonstrated the absence of monomeric populations of PDGFD-GFP-H6, whereas PDGFB-GFP-H6 organized in multiple conformations with different hydrodynamic sizes (Fig. S1C), compatible with the results obtained by DLS (Fig. 1D). Interestingly, the analysis of PDGFD-GFP-H6 revealed the presence of protein nanoparticles with different sizes (Fig. S1D), which were hidden in the broad peak obtained by DLS.

Using electron microscopy, the assembled materials were visualized as discrete entities with sizes compatible to those obtained by DLS (Fig. 1E). A detailed morphometric exploration of selected larger materials in wide and narrow fields revealed a regular, virus-like geometry and a notable structural robustness (Fig. S2).

Envisaging functional analyses of all these materials once exposed to cells and whole bodies, their fluorescence emission was compared to that of the parental GFP-H6 and assessed as a suitable monitoring tool. Noteworthy, all the constructs, in the assembled form, were fluorescent and appropriate for further tracking in cell culture and *in vivo*, in the worst case, reaching 70 % of the GFP-H6 emission (Fig. S3A). In addition, the proteins remained proteolytically stable and soluble in complex culture media (Fig. S3B), indicating that they might be used in further studies. In these analyses, a first internalization screening of the nanoparticles into two PDGFR-β^+ mesenchymal cell types, namely mouse embryonic fibroblasts (MEFs) and mesenchymal stem cells (MSCs), showed a differential uptake (Fig. 2). PDGFB- and PDGFD-based constructs (very especially PDGFD-GFP-H6) showed good cell penetrability at short exposure times (1 h), as determined by GFP immunodetection (Fig. 2A) and further densitometry analysis (Fig. 2B), flow cytometry (Fig. 2C), or by confocal microscopy (Fig. 2D). The smaller PDGFRP1-GFP-H6 and Z09591-GFP-H6 particles, in contrast, rendered internalization values indistinguishable from the background shown by the parental GFP-H6 (Fig. 2B). The amount of detected protein was slightly higher at 1 h than at 24 h (Fig. 2B), probably because of a combination of fast and efficient cell entry and a moderate lysosomal proteolysis of the engulfed material. In this regard, the dotted distribution of the PDGFD-GFP-H6 fluorescence (Fig. 2C) was indicative of an endosomal internalization route. Interestingly, in none of the taken analyses, the exposed cells showed signs of death or cytotoxicity (Fig. 2). For the two internalizing nanoparticles, namely PDGFB-GFP-H6 and PDGFD-GFP-H6, a dose-dependent entry was also demonstrated (Fig. S4), and no plateau was observed, at least up to 1 μM (Fig. S4A, B). This was indicative of the high internalization capacity of both tested nanoparticles and the cell tolerance to the uptake. At 100 nM, the GFP fluorescence of both nanoparticles was widely distributed throughout the cytoplasm of the target cells (Fig. S4C). Again, at high doses of exposed nanoparticles, cells did not exhibit any symptoms of toxicity at different times of exposure to high doses of PDGFB-GFP-H6 (Fig. S5A) or PDGFD-GFP-H6 (Fig. S5B). This was consistent with the intrinsic biocompatibility of proteins as building blocks of se-

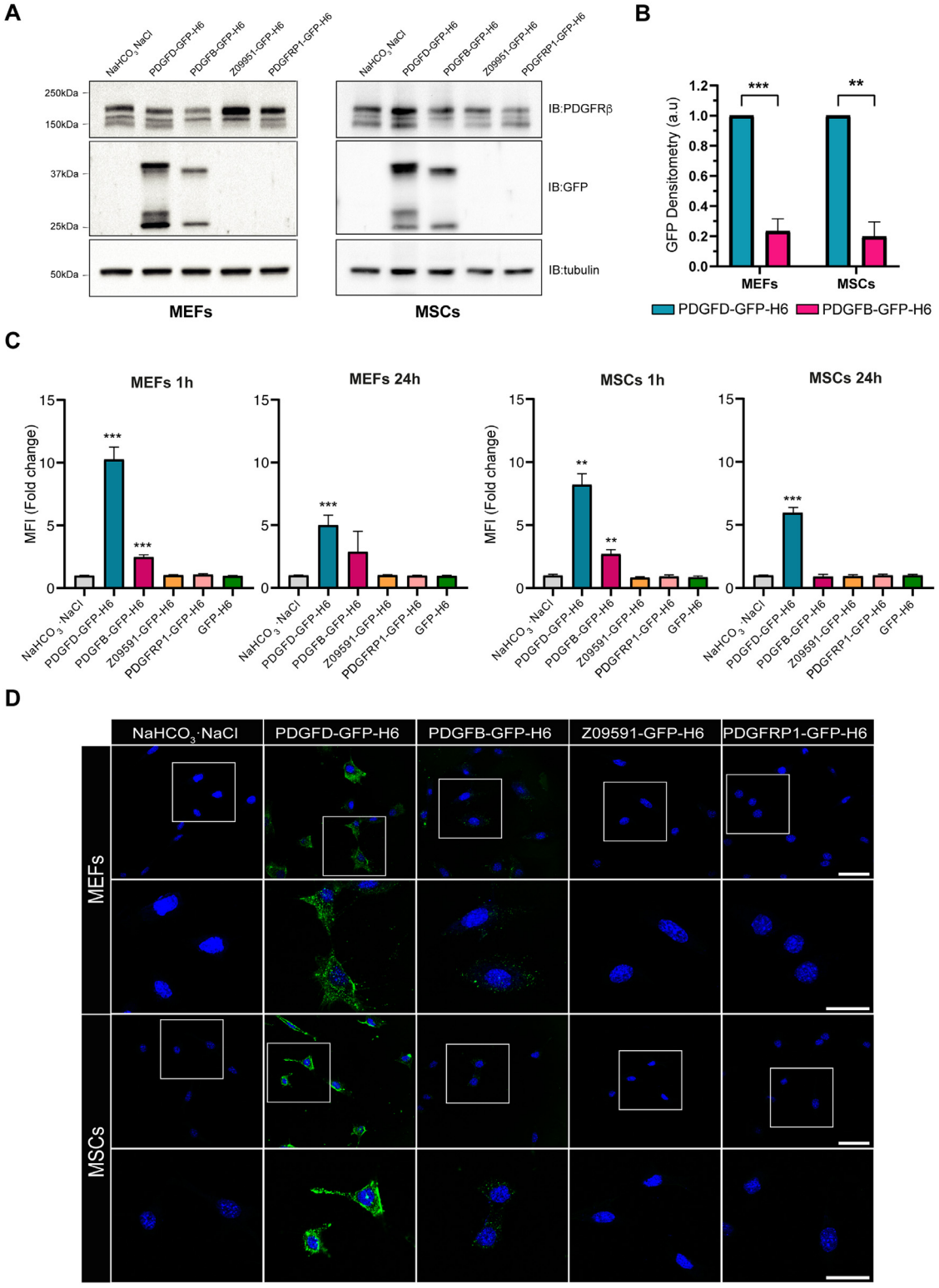

Fig. 2. Internalization of CAFs-directed nanoparticles. Two mesenchymal cell types, mouse embryonic fibroblasts (MEFs) and mesenchymal stem cells (MSCs), were exposed to 100 nM of different nanoparticles. (A) GFP, PDGFR-β and Tubulin immunoblotting of MEFs and MSCs whole cell extracts after 1 h exposure. (B) GFP bands of three independent experiments were quantified to compare internalization between of PDGFB-GFP-H6 and PDGFD-GFP-H6 nanoparticles. (C) Nanoparticle internalization analysed by flow cytometry in MEFs and MSCs upon 1 h or 24 h exposure. Values are expressed as mean fluorescence intensity fold change respect to untreated cells. (D) GFP detection by confocal microscopy upon 1 h exposure, Blue: DAPI. Selected fields are enlarged in the insets for a better visualization. ** $p \leq 0.01$; *** $p \leq 0.001$. Bars size: 50 µm.

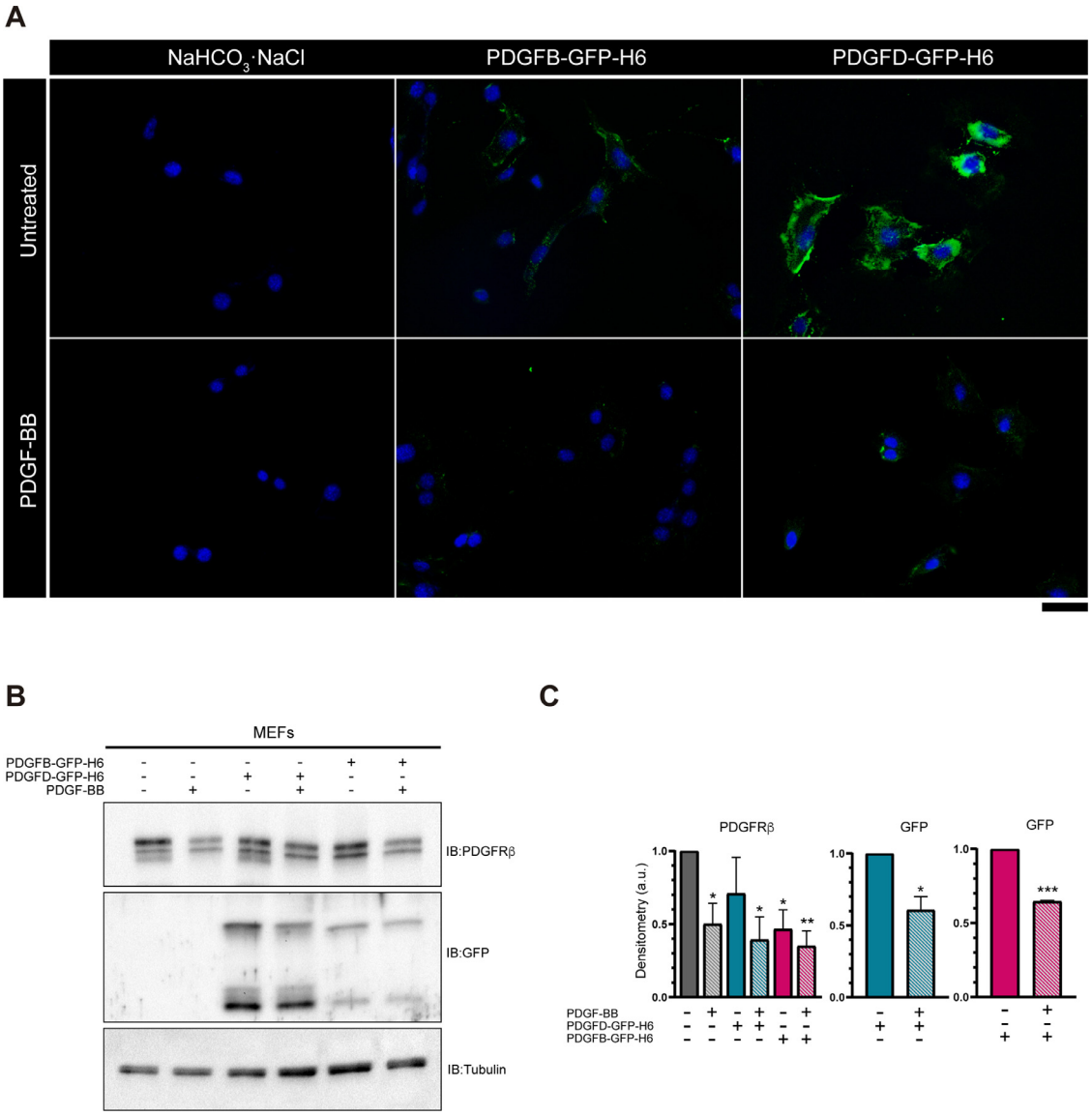

Fig. 3. PDGFR-β is required for internalization of nanoparticles. MEFs were incubated with 50 ng/mL PDGF-BB for 30 min following 100 nM PDGFB-GFP-H6 or PDGFD-GFP-H6 treatment for 1 h. (A) Fixed cells were stained with DAPI and analysed by confocal microscopy. (B) Whole cell extracts were used for detection of PDGFR and GFP, by immunoblotting. Tubulin was used as loading control. (C) Graphs represents densitometry quantification of 3 independent assays. * $p \leq 0.05$; ** $p \leq 0.01$; *** $p \leq 0.001$ Bar size: 50 µm.

lective nanoscale materials, and encouraged us to further analyze the performance of these protein materials, focusing on clinically oriented applications.

In the context of the observed uptake of both tested nanoparticles (Fig. 2), a clear confirmation of the specificity of the process and the requirement of the PDGFR-β as a functional receptor was required. In this regard, the soluble version of the ligand, added before exposure to nanoparticles, blocked their uptake, as determined visually by confocal microscopy (Fig. 3A) or analytically, by immunoblotting (Fig. 3B, C). These competition experiments confirmed that PDGFB-GFP-H6 and PDGFD-GFP-H6 nanoparticles bind to and penetrate target cells upon selective attachment to PDGFR-β. A further confirmation of selectivity was done by immunodetecting GFP in CAFs (MEFs, displaying PDGFRβ) but not in tumor (MC38, not displaying the receptor) cell lines exposed to PDGFD-GFP-H6 (Fig. S6).

To evaluate the *in vivo* performance of PDGFB-GFP-H6 and PDGFD-GFP-H6 nanoparticles, C57BL/6 mice were subcutaneously implanted with the syngeneic colorectal cell line MC38 and MEFs to generate a convenient cancer model, in which PDGFR-β was expressed in the tumor stromal compartment, where activated fibroblasts are located (Fig. 4A). The high homology between human and mouse PDGFR-β (86 %) and PDGFR-β ligands (89 % for PDGFB and 91 % for PDGFD) allowed the testing of the nanoparticles containing human ligands in a mouse model. Two hours after PDGFB-GFP-H6 or PDGFD-GFP-H6 intravenous administration, and in concordance with the *in vitro* data, PDGFD-GFP-H6 nanoparticles accumulated in the tumor (Fig. 4B,C). Concomitantly with its better performance in cell culture (Fig. 2), PDGFD-GFP-H6 showed higher retention in target tissues than PDGFB-GFP-H6 (Fig. 4B,C). The immunohistochemistry detection of the material in the tumor and off-target main organs confirmed the high tumor accumulation and CAFs tumor-selectivity of PDGFD-GFP-H6, which was absent in liver and kidneys (Fig. 4D). In contrast, significant amounts of PDGFB-GFP-H6 nanoparticles, whose internalization into PDGFR-β^+ fibroblasts was moderate (Figs. 2, 4A,B), were unexpectedly retained in the kidneys (Fig. 4D). This observation suggested that PDGFB-GFP-H6, even when showing a promising selectivity in cell

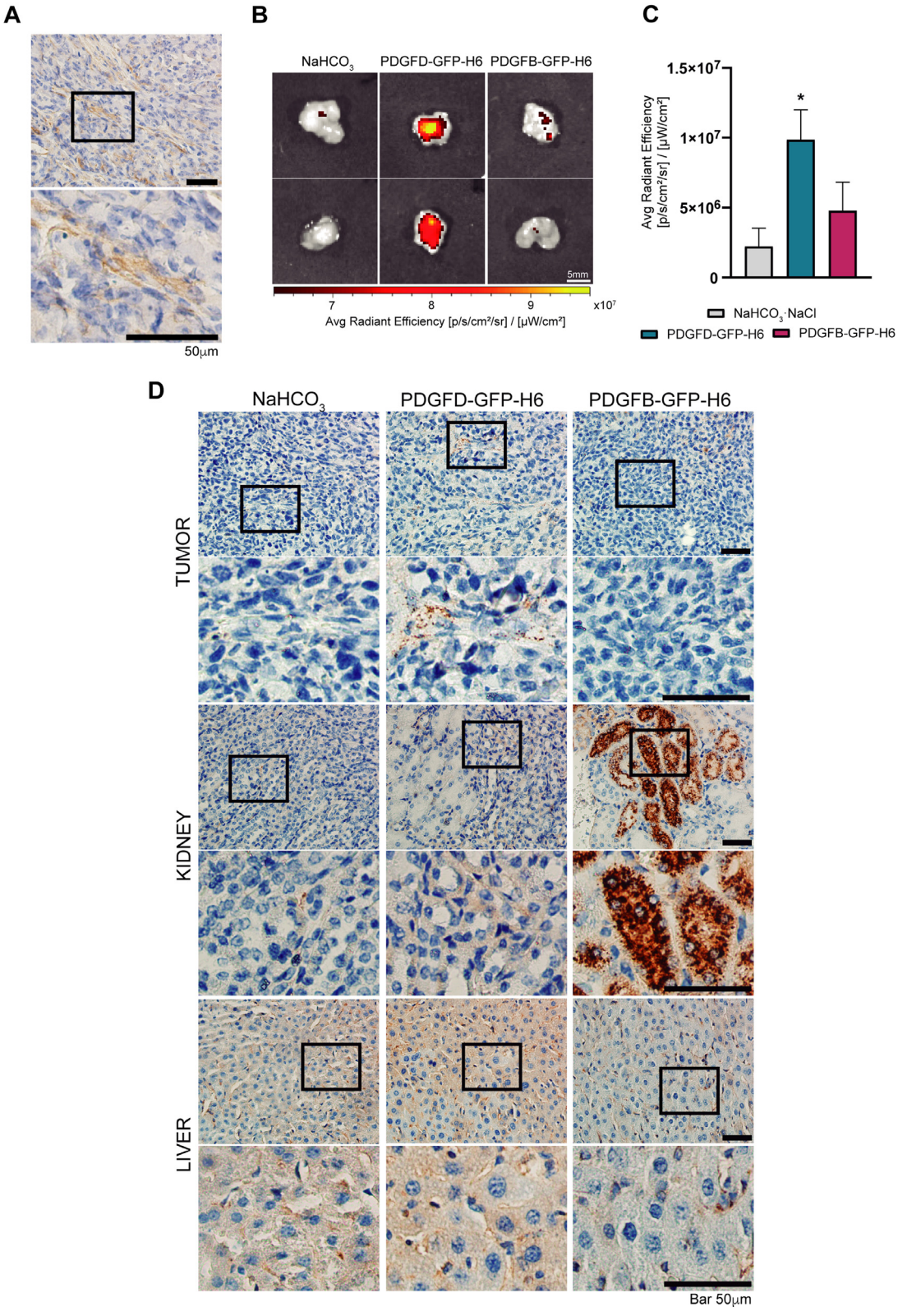

Fig. 4. Biodistribution and *in vivo* uptake of PDGFB-GFP-H6 and PDGFD-GFP-H6. (A) Immunohistochemistry detection of PDGFR-β within tumors. (B) GFP fluorescence detection by IVIS-Spectrum in tumors upon 2 h after PDGFB-GFP-H6 or PDGFD-GFP-H6 administration. (C) Quantification of fluorescence in buffer, PDGFB-GFP-H6 or PDGFD-GFP-H6 treated tumors n=4. (D) Immunohistochemistry against GFP to detect CAFs-targeting nanoparticle in tumor, kidney, and liver of treated mice. * $p \leq 0.05$. Bars size: 50 μm (A,D) and 5 mm (B).

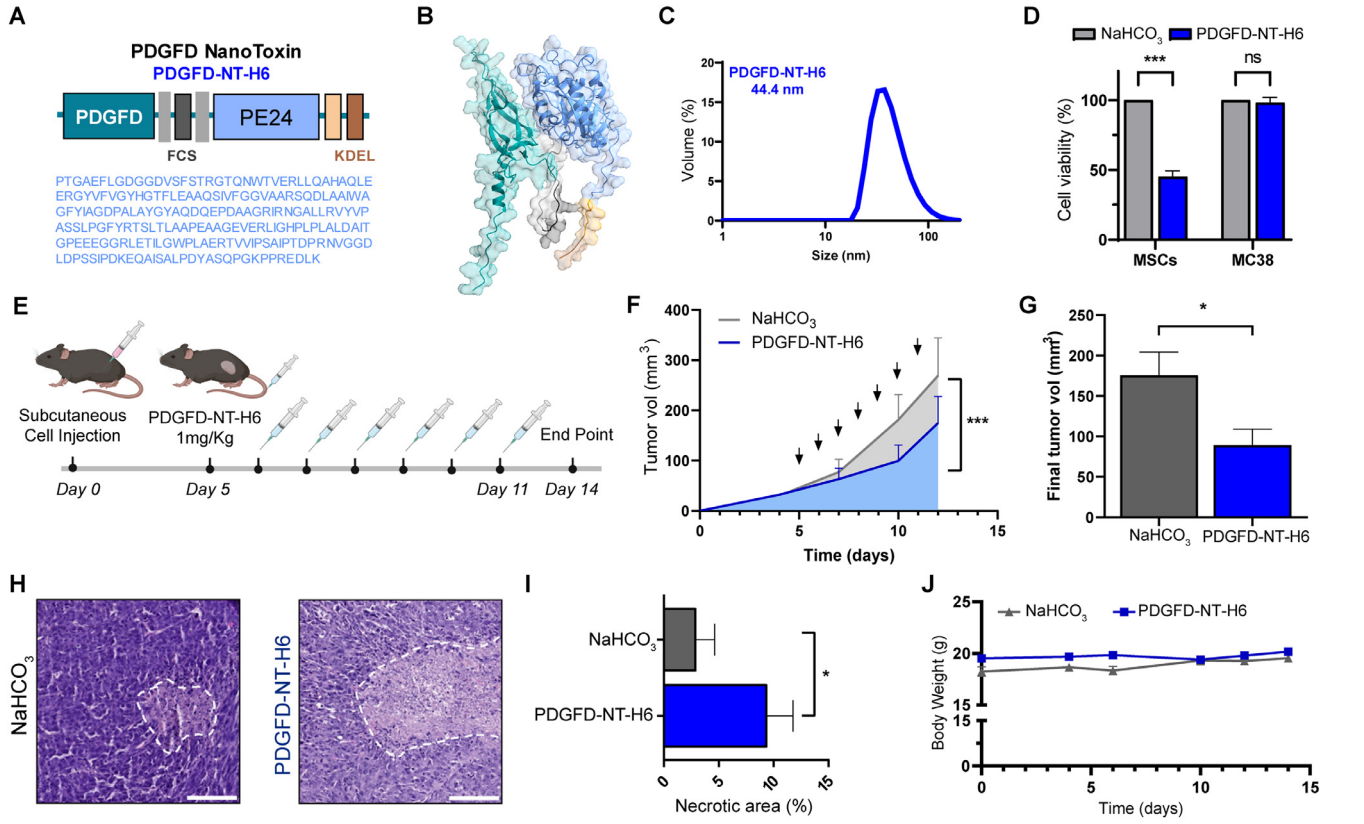

Fig. 5. Antitumoral activity of a PDGFR-β targeted protein nanotoxin. (A) Modular disposition of the nanotoxin PDGFD-NT-H6, from N-terminal (left) to C-terminal (right), based on the catalytic domain of *Pseudomonas aeruginosa* exotoxin A (PE24), whose sequence is depicted in blue. The modular protein also contains the targeting domain PDGFD, flexible linkers (grey boxes), a furin cleavable site (FCS, in black), a H6 tag (orange box) and a subcellular location signal (KDEL tetrapeptide). (B) Three-dimensional model of PDGFD-NT-H6, obtained by AlphaFold approach. Color code as in panel A. (C) Particle size of PDGFD-NT-H6 determined by DLS. Number indicates the mean peak size. Additional data can be found in Table S2. (D) Viability of MSCs and MC38 exposed to 100 nM PDGFD-NT-H6 for 48 h. Untreated cells viability was set as 100 %. (E) Schematic representation of experimental design to assess antitumor activity *in vivo*. (F) *In vivo* measurements of tumor volume throughout the experiment. (G) Tumor volume measured *ex vivo* at the end point after cleaning. (H) Haematoxylin-eosin staining of representative images of necrotic area (dotted line). The scale bars represent 100 µm. (I) Quantification of the necrotic area observed in the tumors of both experimental groups, shown at (H). (J). Mice weight as recorded throughout the experiment. Values are presented as the mean ± SEM. Statistical analysis was performed using the Student's t-test (D) or Mann-Whitney (F,G) *p<0.05, ***p ≤0.001. Tumor volume over time was analysed comparing areas under the curves (AUC).

culture (Fig. 3) might be unsuitable as a PDGFR-β^+ CAFs-targeting agent since its biodistribution was not satisfactory. Although it could be not fully discarded that oligomerization might impair receptor binding, this fact has been not observed in any of the similar modular constructs previously developed for tumor cell targeting *in vivo*, in which the ligand is displayed at the solvent-exposed N-terminus of GFP [81]. However, it has been indeed described that the size of the oligomers or the oligomerization status might deeply affect biodistribution of protein materials with properly displayed cell surface ligands [82]. No signs of systemic toxicity were observed in any of the cases (data not shown).

To test the ability of PDGFD to deliver antitumoral functional domains to PDGFR-β^+ CAFs, a targeted PDGFD-based nanotoxin was designed (PDGFD-NT-H6, Fig. 5A), containing the catalytic domain of *Pseudomonas aeruginosa* exotoxin A (PE24). This protein segment is highly cytotoxic and it has been previously used with success in other types of targeted antitumor protein nanoparticles directed to cancer cells [83,84]. In fact, PE24 has been clinically approved for the treatment of hairy cell leukemia (moxetumomab pasudotox) [85]. Upon recombinant production and purification performed as for PDGFD-GFP-H6 (Supplementary Table 1), the toxin-based multi-domain protein (Fig. 5B) rendered nanoparticles of about 44 nm in diameter (Fig. 5C), coincident with the value (around 50 nm) determined as optimal for endosomal formation and receptor-mediated endocytosis [86–88] and within the size range of the materials suited for the enhanced permeability and retention (EPR) effect [89]. The assembled PDGFD-NT-H6 promoted a significant decrease in the viability of cultured MSCs (but not MC-38 tumor cells) upon incubation for 48 h at 1×10^{-7} M (Fig. 5D). Therefore, an *in vivo* experiment was designed to assess the antitumor activity of the construct (Fig. 5E). C57BL/6 mice were subcutaneously implanted with the syngeneic colorectal cell line, MC38, and MEFs to generate a convenient cancer model. The drug prototype was intravenously administered to 1 mg/kg of PDGFD-NT-H6, daily for up to 7 doses (Fig. 5E). Interestingly, the tumor growth was significantly reduced (Fig. 5F,G), which was associated with induction of necrosis (Fig. 5H,I). The histopathological analysis revealed an increase in the necrotic area within the tumor of PDGFD-NT-H6-treated animals as compared with the buffer-treated control set (Fig. 5H). Interestingly, no signs of side toxicities were observed and in agreement, the body weight of the treated animals evolved as the control group (Fig. 5J). In agreement, the histological examination of liver and kidneys in treated animals revealed again absence of undesired acute toxicities (Fig. S7A), a fact that was further confirmed by unaffected levels of relevant blood markers (Fig. S7B). These data robustly demonstrate the antitumor capability of PDGFD-NT-H6 through the targeting and destruction of PDGFR-β^+ CAFs *in vivo*, that was highly selective as demonstrated by the correct mouse weight evolution.

In summary, by addressing the need to develop non-toxic, non-xenobiotic, and highly selective materials for delivery into tumor-associated PDGFR-β^+ CAFs, we have constructed and characterized

a set of 4 modular proteins, targeting such receptor via alternative peptidic ligands that organize as stable and regular oligomeric nanoparticles (Fig. 1). Ligand-carrying protein oligomers benefit from multiple surface presentations of the ligand in a virus-like fashion [90] and from the cooperativity in the receptor binding and endosome formation [91–93], that results in the final cytoplasmic delivery of the engulfed material. Being protein-based development of cell-targeted nanoparticles a matter of assay and error, PDGFRP1-GFP-H6 and Z09591-GFP-H6 particles failed in an efficient and selective cell binding (Fig. 2). Their small size around 9 nm (Figs. 1, S2) probably contributed to this issue, as larger nanoparticles ranging from ∼ 15 to 80 nm have been repeatedly observed to be as optimal for receptor-dependent cell uptake [8,9,94–97]. Noteworthy, the introduction of these ligands did not promote detectable toxicity upon exposure to target cells (Fig. S5) or off-target toxicity *in vivo* (Figs. 5J, S7). Both PDGFB-GFP-H6 and PDGFD-GFP-H6 nanoparticles, ranging from 16 to 26 nm, selectively targeted and entered PDGFR-β^+ CAFs (Fig. 3), maintaining the fluorescence of the integrated GFP (Figs. 2–4). However, PDGFB-GFP-H6, upon *in vivo* administration in a convenient mouse cancer model, did not show a good biodistribution, being mainly found in the kidney (Fig. 4). Despite its good receptor targeting and selectivity in cell culture (Fig. 3), the protein was unable to perform well *in vivo* regarding the desired biodistribution. This might be attributed to its slight structural instability, as determined by DLS and SEC, as this protein construct is separated into populations of distinct sizes (Table S2, Fig. S3C). In contrast, PDGFD-GFP-H6 resulted in nanoparticles with higher stability and relatively low polydispersion, with a convenient size of around 26 nm and high potency for receptor-dependent specific cell uptake (Figs. 2, 3). Although a small fraction of this protein tends to form small soluble aggregates under specific *in vitro* analytical conditions (Fig. S3D), this fact did not impair protein functionality in cell culture or *in vivo*.

In fact, this nanoparticle was the candidate most efficiently internalized by target cells (Fig. 2), showing an exquisite biodistribution in mice (Fig. 4), with a very selective accumulation in tumoral tissues. This construct was able to target, penetrate and selectively make PDGFR-β^+ CAFs fluorescent (Fig. 4) because of the integrated GFP (Fig. 1), that remained bioactive despite the multiple biological barriers that the construct surpassed after their intravenous administration. The substitution of GFP by a cytotoxic protein drug approved in clinics (Fig. 5A,B) equally resulted into stable nanoparticles (Fig. 5C) that upon *in vivo* administration, promoted an important reduction in tumor growth and induction of necrosis inthe target tissue (Fig. 5F–G), thus validating the developed platform as a potent and original approach for the generation of anticancer drugs.

According to the results shown in the present study, PDGFD-GFP-H6 (and the derived cytotoxic construct) has been fully validated, among the set of starting candidates, as a potent prototype for molecular delivery, imaging and theranostics in cancer through the so far unexplored targeting of CAFs. When a cytotoxic protein is incorporated into the constructs (Fig. 5A), treated animals undergo a significant reduction of tumor growth (Fig. 5F) linked to induction of necrosis (Fig. 5H,I). This must be attributed to a selective destruction of target CAFs, since the tumor cells used to generate the animal model (MC38) do not internalize the nanoparticle (Figs. 5D, S6).

Importantly, this is the first report of the bacterial production and use of PDGFD as a targeting ligand, a fact that opens a spectrum of opportunities for clinical actions. In this context, it was worthy to stress that protein nanoparticles resulting from oligomeric self-assembly can be functionalized through intrinsic, biologically active protein domains [98], by chemically coupling drugs [99], or through combining both strategies [100], opening a spectrum of therapeutic possibilities among which the use of fused protein drugs has been demonstrated here. In particular, chemically attaching conventional small molecular weight drugs to cell-targeted protein-only nanoparticles (based on modular constructs similar to those developed here) is fully feasible and it has rendered interesting prototypes under preclinical development for different types of cancers [27,99,101]. Here, nanoparticles, apart from providing targeting, enlarge the drug size over the renal cut-off and prevent a fast clearance through the kidneys [26]. Importantly, the selective presence of PDGFD-GFP-H6 in tumor (Fig. 4) and specially, the absence of side toxicities observed when administering the highly cytotoxic PDGFD-NT-H6 (Figs. 5, S7) suggest a high level of accumulation. Although experimental data regarding this issue is still missing, similar protein constructs targeted to metastasis cancer stem cells resulted in accumulation levels between 60 and 86 % of the material detectable in the body [29,30], much over the conventional 1-2 % commonly observed in targeted nanomedicines [21]. Although needing experimental confirmation, the results presented here could be in the line of such high values. In addition, the set of results generated in the study totally supports the generic concept of proteins as editable, versatile and biodegradable building blocks suited to construct nanoscale oligomers for clinical purposes. Among other materials under exploration such as lipids, carbon nanotubes, ceramics, metals, and non-protein polymers, that might pose concerns regarding cell toxicity and permanence in the media [102–108], proteins, as main biological molecules, are building blocks convenient for the biofabrication of nanomaterials.

4. Conclusion

Taking concepts from molecular interactomics and protein materials, the modular proteins PDGFD-GFP-H6 and PDGFD-NT-H6 have been designed to self-assemble as protein-only, homo-oligomeric nanoparticles. These materials specifically bind and internalize PDGFR-β^+ stromal fibroblasts, the non-cancer cell type that supports growth, progression and dissemination of high-indicence solid tumors. The delivered GFP or NT (the microbial toxin PE24) are functional upon internalization and either enlighten or destroy target cells depending on the functional protein incoreporated to the building block. The toxin-mediated cell destruction *in vivo* results in significant tumor growth reduction and necrosis, validating the developed platform as promising in oncology. The clinical relevance of targeting cancer-associated fibroblasts and the previous unavailability of molecular tools in this regard, support the proposed concepts as applicable in the molecular delivery, imaging, therapy and theragnostics of cancer by a so far neglected and unconventional strategy.

Declaration of Competing Interest

The authors declare the following financial interests/personal relationships which may be considered as potential competing interests: Antonio Villaverde has patent #NANOCONJUGATES CONTAINING PDGFR-beta LIGANDS AND USES THEREOF. EP22383103 pending to no.

CRediT authorship contribution statement

Eric Voltà-Durán: Conceptualization, Methodology, Formal analysis, Investigation, Writing – review & editing. **Lorena Alba-Castellón:** Conceptualization, Methodology, Formal analysis, Investigation, Writing – review & editing. **Naroa Serna:** Methodology, Formal analysis, Investigation. **Isolda Casanova:** Methodology, Formal analysis, Investigation. **Hèctor López-Laguna:** Methodology, Formal analysis, Investigation. **Alberto Gallardo:** Methodology, Formal analysis, Investigation. **Alejandro Sánchez-Chardi:** Methodol-

ogy, Formal analysis, Investigation. **Antonio Villaverde:** Project administration, Supervision, Resources, Writing – original draft, Writing – review & editing. **Ugutz Unzueta:** Conceptualization, Supervision, Resources, Writing – review & editing. **Esther Vázquez:** Conceptualization, Project administration, Supervision, Resources, Writing – review & editing. **Ramón Mangues:** Conceptualization, Project administration, Supervision, Resources, Writing – review & editing.

Data availability

Raw data can be found at https://doi.org/10.34810/data585.

Acknowledgements

The authors are indebted to Agencia Española de Investigación (AEI) for granting projects on the construction of protein materials of clinical interest (PID2019-105416RB-I00/AEI/10.13039/501100011033 and PDC2022-133858I00/AEI/10.13039/501100011033/ Unión Europea NextGenerationEU/PRTR to EV, and PID2020-116174RB-I00 to AV), to AGAUR for projects SGR2021 00092 to AV and SGR2021 01140 to RM, and to ISCIII for projects P21/00150 to RM and PI20/00400 to UU co-funded by European Regional Development Fund (ERDF, "a way to make Europe"). We also appreciate the support from CIBER -Consorcio Centro de Investigación Biomédica en Red- (CB06/01/0014), Instituto de Salud Carlos III, Ministerio de Ciencia e Innovación and CERCA Programme (Generalitat de Catalunya). Nanoparticle biodistribution was assessed in the Nanotoxicology Unit of the ICTS-141007 Nanbiosis Platform (http://www.nanbiosis.es/portfolio/u18-nanotoxicology-unit/).
U.U. was supported by a Miguel Servet contract (CP19/00028) from ISCIII co-funded by European Social Fund (ESF investing in your future). A.V. received an ICREA ACADEMIA award. E.V.D was supported by a predoctoral fellowship from Ministerio de Ciencia e Innovación, Spain (FPU18/04615), L.A-C by a Postodoctoral fellowship from AECC (Spanish Association Against Cancer, POSTD20070ALBA) and H.L.L by a predoctoral fellowship from AGAUR (2019FI_B00352). Molecular graphics and analyses performed with UCSF ChimeraX, developed by the Resource for Biocomputing, Visualization, and Informatics at the University of California, San Francisco, with support from National Institutes of Health R01-GM129325 and the Office of Cyber Infrastructure and Computational Biology, National Institute of Allergy and Infectious Diseases. The authors want to thank Clara Seira for her technical assistance.

Supplementary materials

Supplementary material associated with this article can be found, in the online version, at doi:10.1016/j.actbio.2023.09.001.

References

[1] H. Sung, J. Ferlay, R.L. Siegel, M. Laversanne, I. Soerjomataram, A. Jemal, F. Bray, Global Cancer Statistics 2020: GLOBOCAN estimates of incidence and mortality worldwide for 36 cancers in 185 countries, CA Cancer J. Clin. 71 (2021) 209–249.
[2] A. Kamb, S. Wee, C. Lengauer, Why is cancer drug discovery so difficult? Nat. Rev. Drug Discov. 6 (2007) 115–120.
[3] A.F. Costa, D. Campos, C.A. Reis, C. Gomes, Targeting glycosylation: a new road for cancer drug discovery, Trends Cancer 6 (2020) 757–766.
[4] B.A. Carneiro, W.S. El-Deiry, Targeting apoptosis in cancer therapy, Nat. Rev. Clin. Oncol. 17 (2020) 395–417.
[5] F. McCormick, Cancer gene therapy: fringe or cutting edge? Nat. Rev. Cancer 1 (2001) 130–141.
[6] B.B.S. Zhou, H. Zhang, M. Damelin, K.G. Geles, J.C. Grindley, P.B. Dirks, Tumour-initiating cells: challenges and opportunities for anticancer drug discovery, Nat. Rev. Drug Discov. 8 (2009) 806–823.
[7] I. Casanova, U. Unzueta, I. Arroyo-Solera, M.V. Cespedes, A. Villaverde, R. Mangues, E. Vazquez, Protein-driven nanomedicines in oncotherapy, Curr. Opin. Pharmacol. 47 (2019) 1–7.
[8] M.J. Mitchell, M.M. Billingsley, R.M. Haley, M.E. Wechsler, N.A. Peppas, R. Langer, Engineering precision nanoparticles for drug delivery, Nat. Rev. Drug Discov. 20 (2021) 101–124.
[9] S. Raj, S. Khurana, R. Choudhari, K.K. Kesari, M.A. Kamal, N. Garg, J. Ruokolainen, B.C. Das, D. Kumar, Specific targeting cancer cells with nanoparticles and drug delivery in cancer therapy, Semin. Cancer Biol. 69 (2019) 166–177.
[10] M.S. Lee, E.C. Dees, A.Z. Wang, Nanoparticle-delivered chemotherapy: old drugs in new packages, Oncology 31 (2017) 198–208.
[11] A. David, Peptide ligand-modified nanomedicines for targeting cells at the tumor microenvironment, Adv. Drug Deliv. Rev. 119 (2017) 120–142.
[12] J. Shi, P.W. Kantoff, R. Wooster, O.C. Farokhzad, Cancer nanomedicine: progress, challenges and opportunities, Nat. Rev. Cancer 17 (2017) 20–37.
[13] S. Tran, P.J. DeGiovanni, B. Piel, P. Rai, Cancer nanomedicine: a review of recent success in drug delivery, Clin. Transl. Med. 6 (2017) 44.
[14] P. Pradeep, P. Kumar, Y.E. Choonara, V. Pillay, Targeted nanotechnologies for cancer intervention: a patent review (2010-2016), Expert Opin. Ther. Pat. 27 (2017) 1005–1019.
[15] O. Cano-Garrido, P. Álamo, L. Sánchez-García, A. Falgàs, A. Sánchez-Chardi, N. Serna, E. Parladé, U. Unzueta, M. Roldán, E. Voltà-Durán, I. Casanova, A. Villaverde, R. Mangues, E. Vázquez, Biparatopic protein nanoparticles for the precision therapy of CXCR4+ cancers, Cancers 13 (2021) 2929.
[16] M. Srinivasarao, C.V. Galliford, P.S. Low, Principles in the design of ligand–targeted cancer therapeutics and imaging agents, Nat. Rev. Drug Discov. 14 (2015) 203–219.
[17] K.C. Tjandra, P. Thordarson, Multivalency in drug delivery–when is it too much of a good thing? Bioconjug. Chem. 30 (2019) 503–514.
[18] Z. Xu, U. Unzueta, M. Roldán, R. Mangues, A. Sánchez-Chardi, N. Ferrer-Miralles, A. Villaverde, E. Vázquez, Formulating tumor-homing peptides as regular nanoparticles enhances receptor-mediated cell penetrability, Mater. Lett. 154 (2015) 140–143.
[19] J. Cossu, F. Thoreau, D. Boturyn, Multimeric RGD-based strategies for selective drug delivery to tumor tissues, Pharmaceutics 15 (2023) 525.
[20] N. Brabez, K. Saunders, K.L. Nguyen, T. Jayasundera, C. Weber, R.M. Lynch, G. Chassaing, S. Lavielle, V.J. Hruby, Multivalent interactions: synthesis and evaluation of melanotropin multimers–tools for melanoma targeting, ACS Med. Chem. Lett. 4 (2013) 98–102.
[21] R. Duncan, R. Gaspar, Nanomedicine(s) under the microscope, Mol. Pharm. 8 (2011) 2101–2141.
[22] S. Wilhelm, A.J. Tavares, Q. Dai, S. Ohta, J. Audet, H.F. Dvorak, W.C.W. Chan, Analysis of nanoparticle delivery to tumours, Nat. Rev. Mater. 1 (2016) 16014.
[23] E. Blanco, H. Shen, M. Ferrari, Principles of nanoparticle design for overcoming biological barriers to drug delivery, Nat. Biotechnol. 33 (2015) 941–951.
[24] L. Yildirimer, N.T. Thanh, M. Loizidou, A.M. Seifalian, Toxicology and clinical potential of nanoparticles, Nano Today 6 (2011) 585–607.
[25] N. Lewinski, V. Colvin, R. Drezek, Cytotoxicity of Nanoparticles, Small 4 (2008) 26–49.
[26] M.V. Cespedes, U. Unzueta, W. Tatkiewicz, A. Sanchez-Chardi, O. Conchillo–Sole, P. Alamo, Z. Xu, I. Casanova, J.L. Corchero, M. Pesarrodona, J. Cedano, X. Daura, I. Ratera, J. Veciana, N. Ferrer-Miralles, E. Vazquez, A. Villaverde, R. Mangues, *In vivo* architectonic stability of fully de novo designed protein-only nanoparticles, ACS Nano 8 (2014) 4166–4176.
[27] M.V. Céspedes, U. Unzueta, A. Aviñó, A. Gallardo, P. Álamo, R. Sala, A. Sánchez-Chardi, I. Casanova, M.A. Mangues, A. Lopez-Pousa, R. Eritja, A. Villaverde, E. Vázquez, R. Mangues, Selective depletion of metastatic stem cells as therapy for human colorectal cancer, EMBO Mol. Med. 10 (2018) e8772.
[28] U. Unzueta, M.V. Céspedes, N. Ferrer-Miralles, I. Casanova, J. Cedano, J.L. Corchero, J. Domingo-Espín, A. Villaverde, R. Mangues, E. Vázquez, Intracellular CXCR4+ cell targeting with T22-empowered protein-only nanoparticles, Int. J. Nanomed. 7 (2012) 4533–4544.
[29] A. Falgàs, V. Pallarès, U. Unzueta, M.V. Céspedes, I. Arroyo-Solera, M.J. Moreno, J. Sierra, A. Gallardo, M.A. Mangues, E. Vázquez, A. Villaverde, R. Mangues, I. Casanova, A CXCR4-targeted nanocarrier achieves highly selective tumor uptake in diffuse large B-cell lymphoma mouse models, Haematologica 105 (2020) 741–753.
[30] E. Medina-Gutiérrez, M.V. Céspedes, A. Gallardo, E. Rioja-Blanco, M.À. Pavón, L. Asensio-Puig, L. Farré, L. Alba-Castellón, U. Unzueta, A. Villaverde, E. Vázquez, I. Casanova, R. Mangues, Novel endometrial cancer models using sensitive metastasis tracing for CXCR4-targeted therapy in advanced disease, Biomedicines 10 (2022) 1680.
[31] N. Serna, L. Sanchez-Garcia, U. Unzueta, R. Diaz, E. Vazquez, R. Mangues, A. Villaverde, Protein-based therapeutic killing for cancer therapies, Trends Biotechnol. 36 (2018) 318–335.
[32] A. Santi, F.G. Kugeratski, S. Zanivan, Cancer associated fibroblasts: the architects of stroma remodeling, Proteomics 18 (2018) 1700167.
[33] D.C. Hinshaw, L.A. Shevde, The tumor microenvironment innately modulates cancer progression, Cancer Res. 79 (2019) 4557–4566.
[34] R. Kalluri, The biology and function of fibroblasts in cancer, Nat. Rev. Cancer 16 (2016) 582–598.
[35] G. Hu, L. Huang, K. Zhong, L. Meng, F. Xu, S. Wang, T. Zhang, PDGFR-beta(+) fibroblasts deteriorate survival in human solid tumors: a meta-analysis, Aging 13 (2021) 13693–13707.

[36] P.J. Asif, C. Longobardi, M. Hahne, J.P. Medema, The role of cancer-associated fibroblasts in cancer invasion and metastasis, Cancers 13 (2021) 4720.
[37] S. Fujino, N. Miyoshi, M. Ohue, Y. Takahashi, M. Yasui, T. Hata, C. Matsuda, T. Mizushima, Y. Doki, M. Mori, Platelet–derived growth factor receptor–β gene expression relates to recurrence in colorectal cancer, Oncol. Rep. 39 (2018) 2178–2184.
[38] E.J. Steller, D.A. Raats, J. Koster, B. Rutten, K.M. Govaert, B.L. Emmink, N. Snoeren, S.R. van Hooff, F.C. Holstege, C. Maas, I.H. Borel Rinkes, O. Kranenburg, PDGFRB promotes liver metastasis formation of mesenchymal-like colorectal tumor cells, Neoplasia 15 (2013) 204–217.
[39] A.A. Jitariu, M. Raica, A.M. Cîmpean, S.C. Suciu, The role of PDGF-B/PDGFR-BETA axis in the normal development and carcinogenesis of the breast, Crit. Rev. Oncol. Hematol. 131 (2018) 46–52.
[40] S. Avril, Y. Dincer, K. Malinowsky, C. Wolff, S. Gundisch, A. Hapfelmeier, M. Boxberg, H. Bronger, K.F. Becker, B. Schmalfeldt, Increased PDGFR-beta and VEGFR-2 protein levels are associated with resistance to platinum-based chemotherapy and adverse outcome of ovarian cancer patients, Oncotarget 8 (2017) 97851–97861.
[41] L. Lu, X. Fu, Z. Li, Y. Qiu, W. Li, Z. Zhou, W. Xue, Y. Wang, M. Jin, M. Zhang, Platelet-derived growth factor receptor alpha (PDGFRα) is overexpressed in NK/T-cell lymphoma and mediates cell survival, Biochem. Biophys. Res. Commun. 504 (2018) 525–531.
[42] Y. Nordby, E. Richardsen, M. Rakaee, N. Ness, T. Donnem, H.R.H. Patel, L.T. Busund, R.M. Bremnes, S. Andersen, High expression of PDGFR-β in prostate cancer stroma is independently associated with clinical and biochemical prostate cancer recurrence, Sci. Rep. 7 (2017) 43378.
[43] S. Szubert, R. Moszynski, D. Szpurek, B. Romaniuk, S. Sajdak, M. Nowicki, S. Michalak, The expression of Platelet-derived Growth factor receptors (PDGFRs) and their correlation with overall survival of patients with ovarian cancer, Ginekol. Pol. 90 (2019) 242–249.
[44] A. Östman, PDGF receptors in tumor stroma: biological effects and associations with prognosis and response to treatment, Adv. Drug Deliv. Rev. 121 (2017) 117–123.
[45] K.C. Valkenburg, A.E. de Groot, K.J. Pienta, Targeting the tumour stroma to improve cancer therapy, Nat. Rev. Clin. Oncol. 15 (2018) 366–381.
[46] N. Effendi, K. Mishiro, K. Shiba, S. Kinuya, K. Ogawa, Development of radiogallium-labeled peptides for platelet-derived growth factor receptor β (PDGFRβ) imaging: influence of different linkers, Molecules 26 (2021) 41.
[47] Y. Yang, Y. Deng, X. Chen, J. Zhang, Y. Chen, H. Li, Q. Wu, Z. Yang, L. Zhang, B. Liu, Inhibition of PDGFR by CP-673451 induces apoptosis and increases cisplatin cytotoxicity in NSCLC cells via inhibiting the Nrf2-mediated defense mechanism, Toxicol. Lett. 295 (2018) 88–98.
[48] N. Papadopoulos, J. Lennartsson, The PDGF/PDGFR pathway as a drug target, Mol. Aspects Med. 62 (2018) 75–88.
[49] N. Serna, V. Pallarès, U. Unzueta, A. Garcia-Leon, E. Voltà-Durán, A. Sánchez-Chardi, E. Parladé, A. Rueda, I. Casanova, A. Falgàs, L. Alba-Castellón, J. Sierra, A. Villaverde, E. Vázquez, R. Mangues, Engineering non-antibody human proteins as efficient scaffolds for selective, receptor-targeted drug delivery, J. Control. Release 343 (2022) 277–287.
[50] H. Lopez-Laguna, E. Volta-Duran, E. Parlade, A. Villaverde, E. Vazquez, U. Unzueta, Insights on the emerging biotechnology of histidine-rich peptides, Biotechnol. Adv. 54 (2022) 107817.
[51] E. Parladé, E. Voltà-Durán, O. Cano-Garrido, J.M. Sánchez, U. Unzueta, H. López-Laguna, N. Serna, M. Cano, M. Rodríguez-Mariscal, E. Vazquez, A. Villaverde, An in silico methodology that facilitates decision making in the engineering of nanoscale protein Materials, Int. J. Mol. Sci. 23 (2022) 4958.
[52] S.T. Wang, B. Minevich, J. Liu, H. Zhang, D. Nykypanchuk, J. Byrnes, W. Liu, L. Bershadsky, Q. Liu, T. Wang, G. Ren, O. Gang, Designed and biologically active protein lattices, Nat. Commun. 12 (2021) 3702.
[53] H. López-Laguna, E. Voltà-Durán, E. Parladé, A. Villaverde, E. Vázquez, U. Unzueta, Insights on the emerging biotechnology of histidine-rich peptides, Biotechnol. Adv. 54 (2021) 107817.
[54] H. Lopez-Laguna, J.M. Sanchez, J.V. Carratala, M. Rojas-Pena, L. Sanchez-Garcia, E. Parlade, A. Sanchez-Chardi, E. Volta-Duran, N. Serna, O. Cano-Garrido, S. Flores, N. Ferrer-Miralles, V. Nolan, A. de Marco, N. Roher, U. Unzueta, E. Vazquez, A. Villaverde, Biofabrication of functional protein nanoparticles through simple His-tag engineering, ACS Sustain. Chem. Eng. 9 (2021) 12341–12354.
[55] S. Gopalakrishnan, J. Xu, F. Zhong, V.M. Rotello, Strategies for fabricating protein films for biomaterial applications, Adv. Sustain. Syst. 5 (2021) 2000167.
[56] J. Shim, C. Zhou, T. Gong, D.A. Iserlis, H.A. Linjawi, M. Wong, T. Pan, C. Tan, Building protein networks in synthetic systems from the bottom-up, Biotechnol. Adv. 49 (2021) 107753.
[57] A. Korpi, E. Anaya-Plaza, S. Valimaki, M. Kostiainen, Highly ordered protein cage assemblies: a toolkit for new materials, Wiley Interdiscip. Rev. Nanomed. Nanobiotechnol. 12 (2020) e1578.
[58] R.V. Ulijn, A. Lampel, Order/disorder in protein and peptide-based biomaterials, Isr. J. Chem. 60 (2020) 1129.
[59] W.A. Hansen, S.D. Khare, Recent progress in designing protein-based supramolecular assemblies, Curr. Opin. Struct. Biol. 63 (2020) 106–114.
[60] X. Xu, X. Chen, J. Li, Natural protein bioinspired materials for regeneration of hard tissues, J. Mater. Chem. B 8 (2020) 2199–2215.
[61] A.J. Najy, J.J. Won, L.S. Movilla, H.R. Kim, Differential tumorigenic potential and matriptase activation between PDGF B versus PDGF D in prostate cancer, Mol. Cancer Res. MCR 10 (2012) 1087–1097.
[62] V. Askoxylakis, A. Marr, A. Altmann, A. Markert, W. Mier, J. Debus, P.E. Huber, U. Haberkorn, Peptide-based targeting of the platelet-derived growth factor receptor beta, Mol. Imaging Biol. 15 (2013) 212–221.
[63] V. Tolmachev, Z. Varasteh, H. Honarvar, S.J. Hosseinimehr, O. Eriksson, P. Jonasson, F.Y. Frejd, L. Abrahmsen, A. Orlova, Imaging of platelet-derived growth factor receptor beta expression in glioblastoma xenografts using affibody molecule 111In-DOTA-Z09591, J. Nucl. Med. 55 (2014) 294–300 official publication, Society of Nuclear Medicine.
[64] J. Strand, Z. Varasteh, O. Eriksson, L. Abrahmsen, A. Orlova, V. Tolmachev, Gallium-68-labeled affibody molecule for PET imaging of PDGFRβ expression *in vivo*, Mol. Pharm. 11 (2014) 3957–3964.
[65] H. López-Laguna, L. Sánchez-García, N. Serna, E. Voltà-Durán, J.M. Sánchez, A. Sánchez-Chardi, U. Unzueta, M. Łoś, A. Villaverde, E. Vázquez, Engineering protein nanoparticles out from components of the human microbiome, Small 16 (2020) e2001885.
[66] V.D. Nguyen, F. Hatahet, K.E. Salo, E. Enlund, C. Zhang, L.W. Ruddock, Pre-expression of a sulfhydryl oxidase significantly increases the yields of eukaryotic disulfide bond containing proteins expressed in the cytoplasm of E.coli, Microb. Cell Fact. 10 (2011) 1.
[67] G. Veggiani, A. de Marco, Improved quantitative and qualitative production of single-domain intrabodies mediated by the co-expression of Erv1p sulfhydryl oxidase, Protein Expr. Purif. 79 (2011) 111–114.
[68] A. Magnusdottir, I. Johansson, L.G. Dahlgren, P. Nordlund, H. Berglund, Enabling IMAC purification of low abundance recombinant proteins from E. coli lysates, Nat. Methods 6 (2009) 477–478.
[69] E. Voltà-Durán, C.G. Olivia, N. Serna, H. López-Laguna, L. Sánchez-García, M. Pesarrodona, A. Sánchez-Chardi, R. Mangues, A. Villaverde, E. Vázquez, U. Unzueta, Controlling self-assembling and tumor cell-targeting of protein-only nanoparticles through modular protein engineering, Sic. China Mater. 63 (2019) 147–156.
[70] J. Jumper, R. Evans, A. Pritzel, T. Green, M. Figurnov, O. Ronneberger, K. Tunyasuvunakool, R. Bates, A. Žídek, A. Potapenko, A. Bridgland, C. Meyer, S.A.A. Kohl, A.J. Ballard, A. Cowie, B. Romera-Paredes, S. Nikolov, R. Jain, J. Adler, T. Back, S. Petersen, D. Reiman, E. Clancy, M. Zielinski, M. Steinegger, M. Pacholska, T. Berghammer, S. Bodenstein, D. Silver, O. Vinyals, A.W. Senior, K. Kavukcuoglu, P. Kohli, D. Hassabis, Highly accurate protein structure prediction with AlphaFold, Nature 596 (2021) 583–589.
[71] E.F. Pettersen, T.D. Goddard, C.C. Huang, E.C. Meng, G.S. Couch, T.I. Croll, J.H. Morris, T.E. Ferrin, UCSF ChimeraX: structure visualization for researchers, educators, and developers, Protein Sci. 30 (2021) 70–82.
[72] R. Batlle, L. Alba-Castellón, J. Loubat-Casanovas, E. Armenteros, C. Francí, J. Stanisavljevic, R. Banderas, J. Martin-Caballero, F. Bonilla, J. Baulida, J.I. Casal, T. Gridley, A. García de Herreros, Snail1 controls TGF-β responsiveness and differentiation of mesenchymal stem cells, Oncogene 32 (2013) 3381–3389.
[73] L. Alba-Castellón, R. Olivera-Salguero, A. Mestre-Farrera, R. Peña, M. Herrera, F. Bonilla, J.I. Casal, J. Baulida, C. Peña, A. García de Herreros, Snail1-dependent activation of cancer-associated fibroblast controls epithelial tumor cell invasion and metastasis, Cancer Res. 76 (2016) 6205–6217.
[74] B. Grum-Schwensen, J. Klingelhofer, C.H. Berg, C. El-Naaman, M. Grigorian, E. Lukanidin, N. Ambartsumian, Suppression of tumor development and metastasis formation in mice lacking the S100A4(mts1) gene, Cancer Res. 65 (2005) 3772–3780.
[75] A. Noel, M.C. De Pauw-Gillet, G. Purnell, B. Nusgens, C.M. Lapiere, J.M. Foidart, Enhancement of tumorigenicity of human breast adenocarcinoma cells in nude mice by matrigel and fibroblasts, Br. J. Cancer 68 (1993) 909–915.
[76] D. Jelinek, E.R. Zhang, A. Ambrus, E. Haley, E. Guinn, A. Vo, P. Le, A.E. Kesaf, J. Nguyen, L. Guo, D. Frederick, Z. Sun, N. Guo, P. Sevier, E. Bilotta, K. Atai, L. Voisin, H.A. Coller, A mouse model to investigate the role of cancer-associated fibroblasts in tumor growth, J. Vis. Exp. JoVE 166 (2020) e61883.
[77] A. Herrera, M. Herrera, L. Alba-Castellon, J. Silva, V. Garcia, J. Loubat–Casanovas, A. Alvarez-Cienfuegos, J. Miguel Garcia, R. Rodriguez, B. Gil, C. Ma Jesus, L. Ma Jesus, J. Ignacio Casal, A.G. de Herreros, F. Bonilla, C. Pena, Protumorigenic effects of Snail-expression fibroblasts on colon cancer cells, Int. J. Cancer 134 (2014) 2984–2990.
[78] H. López-Laguna, J. Sánchez, U. Unzueta, R. Mangues, E. Vázquez, A. Villaverde, Divalent cations: a molecular glue for protein materials, Trends Biochem. Sci. 45 (2020) 992–1003.
[79] U. Unzueta, N. Ferrer-Miralles, J. Cedano, X. Zikung, M. Pesarrodona, P. Saccardo, E. Garcia-Fruitos, J. Domingo-Espin, P. Kumar, K.C. Gupta, R. Mangues, A. Villaverde, E. Vazquez, Non-amyloidogenic peptide tags for the regulatable self-assembling of protein-only nanoparticles, Biomaterials 33 (2012) 8714–8722.
[80] E. Voltà-Durán, J.M. Sánchez, L. Hèctor López, E. Parladé, L. Sánchez-García, A. Sánchez-Chardi, A. de Marco, U. Unzueta, E. Vázquez, A. Villaverde, The spectrum of building block conformers sustains the biophysical properties of clinically-oriented self-assembling protein nanoparticles, Sci. China Mater. 65 (2022) 1662–1670.
[81] F. Rueda, M.V. Céspedes, O. Conchillo-Solé, A. Sánchez-Chardi, J. Seras-Franzoso, R. Cubarsi, A. Gallardo, M. Pesarrodona, N. Ferrer-Miralles, X. Daura, E. Vázquez, E. García-Fruitós, R. Mangues, U. Unzueta, A. Villaverde, Bottom-up instructive quality control in the biofabrication of smart protein materials, Adv. Mater. 27 (2015) 7816–7822 (Deerfield Beach, Fla).
[82] H. López-Laguna, R. Sala, J.M. Sánchez, P. Álamo, U. Unzueta, A. Sánchez-Chardi, N. Serna, L. Sánchez-García, E. Voltà-Durán, R. Mangues,

A. Villaverde, E. Vázquez, Nanostructure empowers active tumor targeting in ligand-based molecular delivery, Part. Part. Syst. Charact. 36 (2019) 1900304.
[83] Y. Núñez, A. Garcia-León, A. Falgàs, N. Serna, L. Sánchez-García, A. Garrido, J. Sierra, A. Gallardo, U. Unzueta, E. Vázquez, A. Villaverde, R. Mangues, I. Casanova, T22-PE24-H6 nanotoxin selectively kills CXCR4-high expressing AML patient cells *in vitro* and potently blocks dissemination *in vivo*, Pharmaceutics 15 (2023) 727.
[84] Z. Zhao, Y. Huang, J. Wang, H. Lin, F. Cao, S. Li, Y. Li, Z. Li, X. Liu, A self-assembling CXCR4-targeted pyroptosis nanotoxin for melanoma therapy, Biomater. Sci. 11 (2023) 2200–2210.
[85] C.F. Nobre, M.J. Newman, A. DeLisa, P. Newman, Moxetumomab pasudotox-tdfk for relapsed/refractory hairy cell leukemia: a review of clinical considerations, Cancer Chemother. Pharmacol. 84 (2019) 255–263.
[86] S. Zhang, J. Li, G. Lykotrafitis, G. Bao, S. Suresh, Size-dependent endocytosis of nanoparticles, Adv. Mater. 21 (2009) 419–424 (Deerfield Beach, Fla).
[87] H. Yuan, S. Zhang, Effects of particle size and ligand density on the kinetics of receptor-mediated endocytosis of nanoparticles, Appl. Phys. Lett. 96 (2010) 033704.
[88] Banerjee A., Berzhkovskii A., Nossal R. Efficiency of cellular uptake of nanoparticles via receptor-mediated endocytosis. arXiv preprint arXiv:14117348 2014.
[89] M. Ikeda-Imafuku, L.L.W. Wang, D. Rodrigues, S. Shaha, Z. Zhao, S. Mitragotri, Strategies to improve the EPR effect: a mechanistic perspective and clinical translation, J. Control. Release 345 (2022) 512–536.
[90] U. Unzueta, M.V. Cespedes, E. Vazquez, N. Ferrer-Miralles, R. Mangues, A. Villaverde, Towards protein-based viral mimetics for cancer therapies, Trends Biotechnol. 33 (2015) 253–258.
[91] J.F. Stefanick, D.T. Omstead, T. Kiziltepe, B. Bilgicer, Dual-receptor targeted strategy in nanoparticle design achieves tumor cell selectivity through cooperativity, Nanoscale (2019).
[92] J. Reichenwallner, A. Thomas, T. Steinbach, J. Eisermann, C.E.H. Schmelzer, F. Wurm, D. Hinderberger, Ligand-binding cooperativity effects in polymer-protein conjugation, Biomacromolecules 20 (2019) 1118–1131.
[93] Y. Li, Y. Wang, G. Huang, J. Gao, Cooperativity principles in self-assembled nanomedicine, Chem. Rev. 118 (2018) 5359–5391.
[94] R.V. Kalaydina, K. Bajwa, B. Qorri, A. Decarlo, M.R. Szewczuk, Recent advances in "smart" delivery systems for extended drug release in cancer therapy, Int. J. Nanomed. 13 (2018) 4727–4745.
[95] P. Debie, C. Lafont, M. Defrise, I. Hansen, D.M. van Willigen, F.W.B. van Leeuwen, R. Gijsbers, M. D'Huyvetter, N. Devoogdt, T. Lahoutte, P. Mollard, S. Hernot, Size and affinity kinetics of nanobodies influence targeting and penetration of solid tumours, J. Control. Release 317 (2020) 34–42.
[96] D. Verma, N. Gulati, S. Kaul, S. Mukherjee, U. Nagaich, Protein based nanostructures for drug delivery, J. Pharm. 2018 (2018) 9285854.
[97] L. Shang, K. Nienhaus, G.U. Nienhaus, Engineered nanoparticles interacting with cells: size matters, J. Nanobiotechnol. 12 (2014) 5.
[98] E. Rioja-Blanco, I. Arroyo-Solera, P. Alamo, I. Casanova, A. Gallardo, U. Unzueta, N. Serna, L. Sanchez-Garcia, M. Quer, A. Villaverde, E. Vazquez, X. Leon, L. Alba-Castellon, R. Mangues, CXCR4-targeted nanotoxins induce GSDME-dependent pyroptosis in head and neck squamous cell carcinoma, J. Exp. Clin. Cancer res. CR 41 (2022) 49.
[99] A. Falgàs, V. Pallarès, U. Unzueta, Y. Núñez, J. Sierra, A. Gallardo, L. Alba–Castellón, M.A. Mangues, P. Álamo, A. Villaverde, E. Vázquez, R. Mangues, I. Casanova, Specific cytotoxic effect of an auristatin nanoconjugate towards CXCR4(+) diffuse large B-cell lymphoma Cells, Int. J. Nanomed. 16 (2021) 1869–1888.
[100] E. Volta-Duran, N. Serna, L. Sanchez-Garcia, A. Avino, J.M. Sanchez, H. Lopez-Laguna, O. Cano-Garrido, I. Casanova, R. Mangues, R. Eritja, E. Vazquez, A. Villaverde, U. Unzueta, Design and engineering of tumor-targeted, dual-acting cytotoxic nanoparticles, Acta Biomater. 119 (2021) 312–322.
[101] V. Pallarès, U. Unzueta, A. Falgàs, A. Aviñó, Y. Núñez, A. García-León, L. Sánchez-García, N. Serna, A. Gallardo, L. Alba-Castellón, P. Álamo, J. Sierra, L. Cedó, R. Eritja, A. Villaverde, E. Vázquez, I. Casanova, R. Mangues, A multivalent Ara-C-prodrug nanoconjugate achieves selective ablation of leukemic cells in an acute myeloid leukemia mouse model, Biomaterials 280 (2022) 121258.
[102] W. Yang, L. Wang, E.M. Mettenbrink, P.L. DeAngelis, S. Wilhelm, Nanoparticle toxicology, Annu. Rev. Pharmacol. Toxicol. 61 (2021) 269–289.
[103] X. Yuan, X. Zhang, L. Sun, Y. Wei, X. Wei, Cellular toxicity and immunological effects of carbon-based nanomaterials, Part. Fibre Toxicol. 16 (2019) 18.
[104] J.B. Raftis, M.R. Miller, Nanoparticle translocation and multi-organ toxicity: a particularly small problem, Nano Today 26 (2019) 8–12.
[105] J. Du, J. Tang, S. Xu, J. Ge, Y. Dong, H. Li, M. Jin, A review on silver nanoparticles-induced ecotoxicity and the underlying toxicity mechanisms, Regul. Toxicol. Pharm. 98 (2018) 231–239.
[106] X. Li, W. Liu, L. Sun, K.E. Aifantis, B. Yu, Y. Fan, Q. Feng, F. Cui, F. Watari, Effects of physicochemical properties of nanomaterials on their toxicity, J. Biomed. Mater. Res. Part A 103 (2015) 2499–2507.
[107] M. Palombo, M. Deshmukh, D. Myers, J. Gao, Z. Szekely, P.J. Sinko, Pharmaceutical and toxicological properties of engineered nanomaterials for drug delivery, Annu. Rev. Pharmacol. Toxicol. 54 (2014) 581–598.
[108] A. Dhawan, V. Sharma, Toxicity assessment of nanomaterials: methods and challenges, Anal. Bioanal. Chem. 398 (2010) 589–605.